$4f^6 \rightarrow 4f^5 5d^1$ absorption spectrum analysis of $Sm^{2+}:SrCl_2$

Mirosław Karbowiak and Agnieszka Urbanowicz
Faculty of Chemistry, University of Wrocław, ul. F. Joliot-Curie 14, 50-383 Wrocław, Poland

Michael F. Reid
Department of Physics and Astronomy, University of Canterbury, Private Bag 4800, Christchurch 8020, New Zealand

(Received 9 February 2007; published 21 September 2007)

The $4f^6 \rightarrow 4f^5 5d^1$ absorption spectrum of the Sm^{2+} ions incorporated in a $SrCl_2$ single crystal was recorded at 4.2 K in the 15 000–45 000 cm^{-1} spectral range. The overall spectrum is very satisfactorily simulated by theoretical calculations performed in the frame of the semi-empirical Hamiltonian model. The calculations enabled the assignment of all bands observed in the spectrum as well as a prediction of some experimentally unobserved transitions in the 45 000–55 000 cm^{-1} region. The rich vibronic structure observed for absorption bands in the 15 000–25 000 cm^{-1} spectral region is dominated by the vibronic progressions in the totally symmetric Sr-Cl stretching mode of ~213 cm^{-1} upon the thirteen zero phonon lines and local vibration modes at ~81 cm^{-1} and ~116 cm^{-1}. This multiphonon vibronic spectrum is very well reproduced by the model calculation.

DOI: 10.1103/PhysRevB.76.115125 PACS number(s): 71.70.Ch, 78.20.Bh, 78.40.−q

I. INTRODUCTION

The absorption lines observed for lanthanide (Ln) ions in the IR, Vis, UV and VUV spectral ranges, result from the intraconfigurational $nf^N \rightarrow nf^N$ and interconfigurational $nf^N \rightarrow nf^{N-1}(n+1)d^1$ transitions. The $nf^N \rightarrow nf^N$ transitions have been a subject of intense studies over the past several decades, that have been initially stimulated by the development of solid state lasers, and later also by other numerous applications which may be based on the optical properties of lanthanides. As the result of these efforts, the energy levels of the nf^N configuration for Ln^{3+} have been relatively well characterized and understood in terms of theoretical models.[1–3]

On the other hand, the number of papers dealing with the interconfigurational $nf^N \rightarrow nf^{N-1}(n+1)d^1$ transitions of the lanthanide ions is significantly smaller than that for *f-f* transitions. Moreover, in most cases, the structure of the observed $4f^N \rightarrow 4f^{N-1}5d^1$ transitions has been rationalized in the simple one-electron model, suitable for Ce^{3+} ions only,[4,5] or with the assumption that the excited configurations were formed by a coupling of the 5*d* orbitals, split by the crystal-field, with the $4f^{N-1}$ core electrons and lattice vibrations.[6–8] However, recently, a growing interest in rare-earths spectroscopy in the vacuum ultraviolet range may be observed. It mostly results from a search for new efficient luminescence materials under VUV excitation. Owing to the occurrence of *f-d* transitions in this spectral region, development of theoretical models for their interpretation is required.

The *f-d* transitions of metal ions impurities embedded in ionic hosts can be successfully rationalized by the *ab initio* theoretical calculations.[9,10] However, such calculations are usually rather demanding and difficult to perform by nonspecialist. Far more straightforward is a phenomenological theoretical model for the calculation of the $4f^{N-1}5d^1$ energy levels, proposed by Reid *et al.*,[11] which extends the established model for the $4f^N$ configuration by including crystal-field and spin-orbit interactions for the 5*d* electron as well as the Coulomb interactions between the 4*f* and 5*d* electrons.

This approach was successfully applied for analysis of the excitation spectra of Ln^{3+} ions in $LiYF_4$, CaF_2, and YPO_4 (Refs. 12 and 13) as well as absorption spectra of U^{3+} ions in $LiYF_4$ (Ref. 14), Cs_2NaYCl_6 (Ref. 15) and $SrCl_2$ (Ref. 16). More recently this model was used for simulation of *f-d* spectra of $Eu^{2+}:SrCl_2$ (Ref. 17). It was shown in Refs. 15 and 16 that the suitability of U^{3+} ions for the *f-d* transition studies, lays in appearance of first absorption bands as low as ~15 000 cm^{-1}above the ground $^4I_{9/2}$ state, which makes the $5f^3 \rightarrow 5f^2 6d^1$ transitions more accessible experimentally as compared, for example, with Ln^{3+} ions, for which the $4f^N \rightarrow 4f^{N-1}5d^1$ absorption bands are observed in the UV and VUV regions. The similar shift of *f-d* bands towards lower energy spectral regions is observed when Ln^{3+} ions become reduced to the divalent form. In addition, the crystal-field strength is for Ln^{2+} ions about two times weaker compared to U^{3+} ions, which results in the smaller energy separation between e_g and t_{2g} states (in O_h symmetry), and makes the absorption transition to the latter one observable in the UV spectral region. This is a noteworthy advantage of Sm^{2+} ions over U^{3+} ions, for which the analysis was limited, in the case of the $SrCl_2$ host, to the well resolved transitions to e_g states only, whereas the transitions to the t_{2g} levels were observed in the absorption spectrum as broad and unstructured bands.[16]

The absorption spectrum of $Sm^{2+}:SrCl_2$ measured at 4.2 K in the 710–380 nm range has been reported by Axe and Sorokin.[18] In this paper we present the low-temperature absorption spectra recorded in the region extended to 220 nm, which cover the wavelength range of transitions to the $4f^5 5d(t_{2g})^1$ states, not reported in Ref. 18. From analysis of the vibronic spectrum a number of electronic origins was determined. The theoretical energy levels and transition intensities were calculated using parametric Hamiltonian model and the overall electronic absorption spectrum was very satisfactorily simulated. The pronounced fine vibronic structure observed in the spectrum is adequately reproduced using the theory of multiphonon vibronic coupling to electronic transitions.

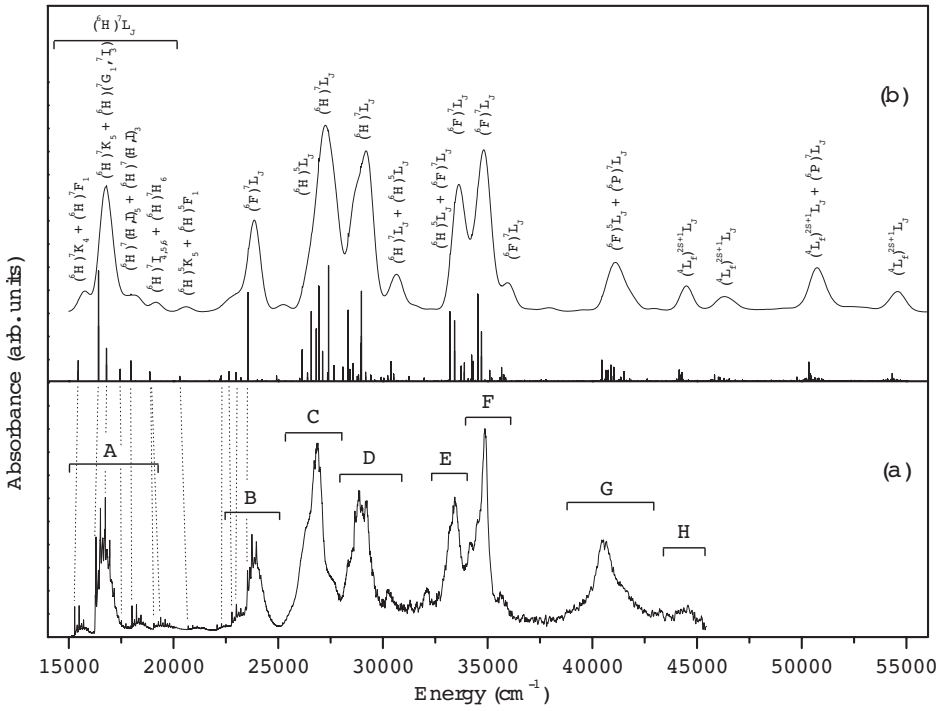

FIG. 1. (a) Survey of the $4f^6 \rightarrow 4f^5 5d^1$ absorption spectrum at 4.2 K of $Sm^{2+}:SrCl_2$. The observed transitions are grouped into bands labeled arbitrary with capital letters A–H. (b) The overall spectrum calculated by using Hamiltonian of Eq. (1) and parameters of Table II. The sticks at the bottom indicate the calculated positions of the zero-phonon lines, with the heights proportional to the predicted intensities. The largest component of the eigenvectors is indicated for the terminal levels of the $4f^5 5d^1$ configuration with the highest predicted $^7F_0 \rightarrow (S_f L_f)$ *SLJ* transition intensity within a given absorption band. The vertical dot lines connect the calculated and experimental positions of ZP lines.

II. EXPERIMENTAL SECTION

Samarium(II) doped single crystals of $SrCl_2$ with a nominal 0.12 at.% samarium concentration were grown by the Bridgman method. Dry $SrCl_2$ powder was mixed with appropriate amount of $SmCl_3$, placed in a vitreous carbon crucible and sealed under argon in silica ampoules. The ampoule was lowered through the vertical furnace at 1195 K, at a rate of 4 mm/h. The doped single crystals were cut and polished under dry paraffin oil.

The absorption spectra were recorded on a Cary-50 UV-Vis-NIR spectrophotometer in the 10 000–50 000 cm^{-1} range. An Oxford Instrument model CF1204 cryostat was used for low-temperature measurements.

III. RESULTS

A. Absorption spectrum

In Fig. 1(a) a 4.2 K survey absorption spectrum of $Sm^{2+}:SrCl_2$ is shown. In the 15 000–25 000 cm^{-1} range the spectrum is identical to that presented by Axe and Sorokin.[18] Absorption bands observed in this range result from transitions from the $4f^6(^7F_0)$ ground multiplet to the $4f^5 5d(e_g)^1$ crystal-field levels of Sm^{2+} ions. As results form theoretical calculations, presented in Section III B, the most intense bands observed at the energy region above 25 000 cm^{-1}, not reported in Ref. 18, should be assigned as transitions to the $4f^5 5d(t_{2g})^1$ levels of Sm^{2+}.

Figure 2 shows a high-resolution absorption spectrum recorded at 4.2 K for $Sm^{2+}:SrCl_2$ in the spectral region corresponding to the $4f^6(^7F_0) \rightarrow 4f^5 5d^1(e_g)^1$ transitions. The most prominent feature of the spectrum is the ~213 cm^{-1} vibronic progression that arises from the totally symmetric $\nu_1(a_{1g})$ stretch of the $SmCl_8^{6-}$ moiety. The lowest-energy zero-phonon (ZP) line is distinctly observable at 15 280 cm^{-1} (line 1). For this line, the $\nu_1(a_{1g})$ progression extends through four quanta. The magnified view of the vibronic massive accompanying the 15 280 cm^{-1} ZP line is given in the inset of Fig. 2. The ZP line is the sharpest and the other lines become successively broader for higher energy members of the progression. The same holds true for other bands in the spectrum. From the analysis of the spectrum two other vibrational energies, at ~81 cm^{-1} and ~116 cm^{-1}, can be deduced, labeled in the inset of Fig. 2 as ν_2 and ν_3, respectively. These phonon lines also serve as an origin for the 213 cm^{-1} vibronic progression. Some additional very weak phonon lines, marked in the inset of Fig. 2 with asterisks, can be discerned at 133, 165, and 189 cm^{-1}.

The intense massive observed between 16 250 and 17 500 cm^{-1} is composed of vibronic bands coupled to three ZP lines at 16 267, 16 297, and 16 741 cm^{-1}. The next ZP lines could be localized readily at 17 514, 18 018, 19 068, and 19 381 cm^{-1}. In Fig. 2, the determined positions of the zero-phonon transitions are marked with arrows, whereas the $\nu_1(a_{1g})$ vibronic progressions coupled to each of the ZP line are indicated by dotted vertical lines.

The careful analysis of the spectrum enabled the determination of positions of thirteen zero-phonon lines in the 15 000–25 000 cm^{-1} region. The energies of all ZP lines and the accompanying them vibronic satellites, corresponding to the $\nu_1(a_{1g})$ mode, identified in this region of absorption spectrum are listed in Table I. Numbers in column 1 of this table correspond to the line labels in Fig. 2. The remaining lines, not listed in Table II and marked in Fig. 2 with circles, may

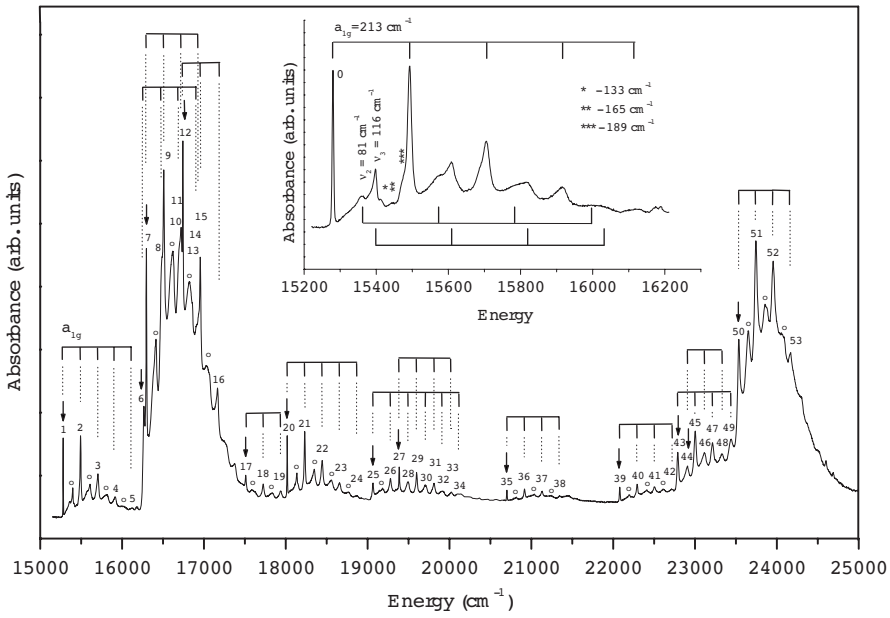

FIG. 2. Absorption spectrum recorded at 4.2 K for the $Sm^{2+}:SrCl_2$ single crystal in the $4f^6(^7F_0) \rightarrow 4f^5 5d^1(e_g)^1$ transition range. The zero-phonon lines are marked with arrows, whereas the vibronic progressions that arise from the $\nu_1(a_{1g})$ mode are indicated by dotted lines. The $\nu_2 = 81\ cm^{-1}$ and $\nu_3 = 116\ cm^{-1}$ phonon lines and the nth order progressions built on them are indicated by circles. The inset shows the lowest energy band in greater detail. The displacements from the 15 280 cm^{-1} origin are marked and the progressions in $\nu_1(a_{1g})$, ν_2 and ν_3 are indicated. Some additional very weak phonon lines are marked with asterisks.

be correspondingly assigned as the minor ν_2 or ν_3 phonon lines and the nth order progressions built on them.

B. Calculation of $4f^5 5d^1$ energy levels and $4f^6 \rightarrow 4f^5 5d^1$ transition line strengths

Energy levels and the $4f^6 \rightarrow 4f^5 5d^1$ transition intensities of Sm^{2+} in $SrCl_2$ were calculated using a theoretical model for nf^N energy levels extended for interactions related with the presence of $(n+1)d$ electron, developed by Reid *et al.*[11] It is assumed, that for the excited $nf^{N-1}(n+1)d^1$ configuration the nf^{N-1} core experiences the same interactions as the nf^N configuration. These interactions are: Coulomb interaction between nf electrons [parametrized by $F^k(ff)$], spin-orbit interaction [parametrized by $\zeta_{4f}(ff)$], two-electron correlation corrections to the Coulomb repulsions [parametrized by $\alpha(ff)$, $\beta(ff)$, and $\gamma(ff)$], three-electron correlations [parametrized by $T^i(ff)$], electrostatically correlated spin-orbit interactions [parametrized by $P^k(ff)$] as well as spin-spin and spin-other orbit interactions [parametrized by $M^j(ff)$]. However, due to the presence of d-electron atomic part of Hamiltonian is supplemented by the spin-orbit interactions for the $(n+1)d$ electron, parametrized by $\zeta(dd)$, and the Coulomb interactions between the $(n+1)d$ electron and the nf^{N-1} electrons, parametrized by direct $F^k(fd)$ $(k=2,4)$ and exchange $G^j(fd)(j=1,3,5)$ Slater parameters. The crystal-field (CF) interactions of the nf^{N-1} and $(n+1)d$ electrons with the lattice are parametrized by $B_q^k(ff)$ $(k=2,4,6)$ and $B_q^k(dd)$ $(k=2,4)$, respectively, with value of q restricted by site symmetry. The difference in energy between excited $nf^{N-1}(n+1)d^1$ and ground nf^Nconfiguration is parametrized by $\Delta_E(fd)$. Then, the complete Hamiltonian for $nf^{N-1}(n+1)d^1$ configuration may be written as

$$\hat{H} = E_{\text{avg}} + \sum_{k=2,4,6} F^k(ff)\hat{f}_k(ff) + \zeta_{4f}(ff)\hat{A}_{SO}(ff) + \alpha(ff)\hat{L}(\hat{L}+1) + \beta(ff)\hat{G}(G_2) + \gamma(ff)\hat{G}(R_7) + \sum_{k=2,4,6} P^k(ff)\hat{p}_k(ff) + \sum_{k,q} B_q^k(ff)C_q^{(k)}(ff) + \Delta_E(fd)\delta_E(fd) + \sum_{k=2,4} F^k(fd)f_k(fd) + \sum_{j=1,3,5} G^j(fd)g_j(fd) + \zeta(dd)A_{SO}(dd) + \sum_{k,q} B_q^k(dd)C_q^{(k)}(dd). \quad (1)$$

Energy levels for the $4f^5 5d^1$ configuration of Sm^{2+} were calculated by diagonalization of the above Hamiltonian, using f-shell programs.[19]

The initial values of the Hamiltonian parameters for the $4f^5$ core electrons were estimated on the basis of the parameters for the $4f^5$ configuration of Sm^{3+} (Ref. 20). As the initial values of CF interaction parameters for the $4f$ and $5d$ electrons the half values of $B_0^4(ff)$, $B_0^6(ff)$, and $B_0^4(dd)$ parameters reported for $Eu^{3+}:SrF_2$ (Ref. 21) and $Ln^{3+}:CaF_2$ (Ref. 12) were assumed, respectively. The parameters for Coulomb interactions between the $4f^5$ electrons and $5d^1$ electron as well as for spin-orbit interactions of $5d$ electron were obtained from free-ion *ab initio* calculations using standard atomic computer programs.[22] However, due to the delocalization of the $4f$ and $5d$ electrons over the ligands (the nephelauxetic effect) these interaction parameters for Sm^{2+} ion embedded in crystalline host are expected to be significantly smaller compared to the free-ion values. In accordance with this expectation, the values initially reduced to 65% of calculated values were used at a starting point of the calculations.

The calculations were performed with $F^2(ff)$, $\zeta(ff)$, $B_0^4(ff)$, $B_0^6(ff)$, $\Delta_E(fd)$, $F^2(fd)$, $G^1(fd)$, $\zeta(dd)$, and $B_0^4(dd)$

TABLE I. Positions and assignments of the zero-phonon (ZP) and vibronic lines corresponding to the ~213 cm^{-1} $\nu_1(a_{1g})$ totally symmetric stretch of the $SmCl_8^{6-}$ moiety, observed in the 15 250–23 550 cm^{-1} absorption transition range of the Sm^{2+} ion in a $SrCl_2$ single crystal.

Line, Fig. 2[a]	Assignment	Line position (cm^{-1})	Line, Fig. 2[a]	Assignment	Line position (cm^{-1})
1	ZP(1)	15280	28	ZP(7)+2ν_1	19068+426
2	ZP(1)+ν_1	15280+213	29	ZP(8)+ν_1	19381+225
3	ZP(1)+2ν_1	15280+426	30	ZP(7)+3ν_1	19068+635
4	ZP(1)+3ν_1	15280+639	31	ZP(8)+2ν_1	19381+435
5	ZP(1)+4ν_1	15280+852	32	ZP(7)+4ν_1	19068+846
6	ZP(2)	16267	33	ZP(8)+3ν_1	19381+640
7	ZP(3)	16297	34	ZP(7)+5ν_1	19068+1070
8	ZP(2)+ν_1	16271+209	35	ZP(9)	20705
9	ZP(3)+ν_1	16300+213	36	ZP(9)+ν_1	20705+215
10	ZP(2)+2ν_1	16271+429	37	ZP(9)+2ν_1	20705+416
11	ZP(3)+2ν_1	16300+420	38	ZP(9)+3ν_1	20705+641
12	ZP(4)	16741	39	ZP(10)	22075
13	ZP(2)+3ν_1	16271+637	40	ZP(10)+ν_1	22075+221
14	ZP(4)+ν_1	16741+214	41	ZP(10)+2ν_1	22075+421
15	ZP(4)+2ν_1	16741+426	42	ZP(10)+3ν_1	22075+631
16	ZP(4)+3ν_1	16741+638	43	ZP(11)	22778
17	ZP(5)	17514	44	ZP(12)	22910
18	ZP(5)+ν_1	17514+211	45	ZP(11)+ν_1	22778+219
19	ZP(5)+2ν_1	17514+423	46	ZP(12)+ν_1	22910+212
20	ZP(6)	18018	47	ZP(11)+2ν_1	22778+426
21	ZP(6)+ν_1	18018+213	48	ZP(12)+2ν_1	22910+422
22	ZP(6)+2ν_1	18018+432	49	ZP(11)+3ν_1	22778+669
23	ZP(6)+3ν_1	18018+638	50	ZP(13)	23530
24	ZP(6)+4ν_1	18018+828	51	ZP(13)+ν_1	23535+222
25	ZP(7)	19068	52	ZP(13)+2ν_1	23535+424
26	ZP(7)+ν_1	19068+216	53	ZP(13)+3ν_1	23525+624
27	ZP(8)	19381			

[a]Numbers in these columns correspond to the line labels in Fig. 2.

treated as optimized parameters. The constant empirical ratios: $F^4(ff)/F^2(ff)=0.720$ and $F^6(ff)/F^2(ff)=0.500$, typical for the $4f^5$ configuration of Sm^{3+} (Ref. 20), were retained. The relations between $F^2(fd)$ and $F^4(fd)$, $G^1(fd)$, and $G^3(fd)$as well as between $G^1(fd)$ and $G^5(fd)$ parameters were constrained by the Cowan's code calculated fixed ratios: $F^4(fd)/F^2(fd)=0.487$, $G^3(fd)/G^1(fd)=0.861$, and $G^5(fd)/G^1(fd)=0.669$. All other parameters were not allowed to vary in the optimization procedure.

The parameters of the Hamiltonian were optimized by changing their values within certain physically justified ranges, calculating of the energy levels and transition intensities, and repeating this procedure until the best agreement was obtained between the calculated and experimental spectrum. The final values for parameters of Hamiltonian of Eq. (2) are listed in Table II.

The transitions from the $4f^6$ to the $4f^55d^1$ configuration are electric-dipole allowed and the appropriate matrix elements for the transitions can be calculated using expressions given in Ref. 17. In the calculations, the approximation was made that the intensity of the ZP line is proportional to the total electric dipole transition line strength, multiplied by the transition energy. The calculated energy levels as well as predicted relative transition intensities of zero-phonon lines are shown graphically by the vertical sticks at the bottom of Fig. 1(b).

IV. DISCUSSION

A. $4f^6 \rightarrow 4f^55d^1$ transitions

Strontium chloride crystallizes in a fluorite-type structure and is isostructural with CaF_2. In this host Sm^{2+} ions substitute for Sr^{2+} ions at site of O_h symmetry, and since Sm^{2+} ions possess the same charge and similar ionic radius (127 pm) as Sr^{2+} (126 pm) (Ref. 23) no lattice distortions are expected for $Sm^{2+}:SrCl_2$ crystals.

The CF calculations show that the $4f^55d^1$ configuration extends throughout about 150 000 cm^{-1}. However, only for transitions to levels positioned approximately 150 000 cm^{-1} above the lowest $4f^55d^1$ level, the predicted intensities are large enough to permit them to be observable in absorption. Since the first $4f^6 \rightarrow 4f^55d^1$ absorption line of the Sm^{2+} ion

TABLE II. Energy parameters for the $4f^5 5d^1$ configuration of Sm^{2+} in $SrCl_2$. The initial values of parameters for the splitting of the $4f^5$ core are obtained from the literature (Ref. 18) (mean free-ion values for $4f^5$ configuration of Sm^{3+}). Starting parameters for *f-d* interactions were calculated using Cowan's code (Ref. 22). The values in square brackets were not allowed to vary in the optimization procedure.

Parameter	Value (cm^{-1})
$F^2(ff)$	80000
$F^4(ff)$[a]	57600
$F^6(ff)$[a]	40000
$\zeta_{4f}(ff)$	1100
$\alpha(ff)$	[20.50]
$\beta(ff)$	[−616]
$\gamma(ff)$	[1565]
$M^0(ff)$[b]	[2.38]
$P^2(ff)$[b]	[336]
$T^2(ff)$	[282]
$T^3(ff)$	[26]
$T^4(ff)$	[71]
$T^6(ff)$	[−257]
$T^7(ff)$	[314]
$T^8(ff)$	[328]
$B_0^4(ff)$[c]	−710
$B_0^6(ff)$[c]	215
$\Delta_E(fd)$	9506
$F^2(fd)$	14900
$F^4(fd)$[d]	7256
$G^1(fd)$	7200
$G^3(fd)$[d]	6200
$G^5(fd)$[d]	4817
$\zeta(dd)$	860
$B_0^4(dd)$[e]	−20500

[a]The $F^4(ff)$ and $F^6(ff)$ parameters were constrained by the empirical fixed ratios: $F^4(ff)/F^2(ff)=0.720$ and $F^6(ff)/F^2(ff)=0.500$, taken from Ref. 18.

[b]The $M^2(ff)$, $M^4(ff)$, $P^4(ff)$, and $P^6(ff)$ parameters were constrained by the Hartree-Fock determined fixed ratios: $M^2(ff)=0.59\ M^0(ff)$, $M^4(ff)=0.38\ M^0(ff)$, $P^4(ff)=0.75\ P^2(ff)$, and $P^6(ff)=0.5,\ P^2(ff)$.

[c]$B_4^4(ff)=\sqrt{5/14}B_0^4(ff)=-424\ cm^{-1}$, $B_4^6(ff)=-\sqrt{7/2}B_0^6(ff)=-402\ cm^{-1}$.

[d]The $F^4(fd)$, $G^3(fd)$, and $G^5(fd)$ parameters were constrained by the fixed ratio: $F^4(fd)/F^2(fd)=0.487$, $G^3(fd)/G^1(fd)=0.861$, and $G^5(fd)/G^1(fd)=0.669$, calculated using Cowan's code.[22]

[e]$B_4^4(dd)=\sqrt{5/14}B_0^4(dd)=-12251\ cm^{-1}$.

in a $SrCl_2$ crystal appears at energy as low as 15 280 cm^{-1}, we were able to record experimentally the most of the observable transitions predicted by the theory. Only some lower intensity bands, resulting from transitions to the $(^6P)^7L_J$ and the quartet $(^4L_f)^{2S+1}L_J$ states, predicted by CF calculations at energy between 45 000 and 55 000 cm^{-1} (Fig. 1), stay beyond the range achievable with our spectrophotometer. To our knowledge, transitions to the $4f^5 5d(t_{2g})^1$ levels of Sm^{2+}, as well as to other levels positioned above 25 000 cm^{-1}, have never been reported in the literature. Thus, the well resolved absorption bands observed in the broad spectral region and encompassing the significant part of the theoretically allowed transitions, should be a firm basis for the reliable determination of Hamiltonian parameters. Moreover, the presence of fine vibronic structure observed clearly for the lower energy bands (Fig. 2) allows for detailed analysis of vibronic coupling.

In the very rough approximation, for the rationalization of the structure of the spectrum one may applied a qualitative reasoning, assuming a superposition of the multiplet structure of the $4f^5$ core on the $5d^1$ crystal-field levels. The Sm^{2+} ion in the $SrCl_2$ crystal has a cubic eightfold coordination, and the crystal field splits the $5d^1$ electronic state into an e_g lower and a t_{2g} upper state. The e_g level of Γ_{8g} symmetry is not split by a spin-orbit interaction, whereas the t_{2g} state is split into a Γ_{8g} degenerate quartet and Γ_{7g} Kramer's doublet. Thus the two lowest groups of the energy levels, denoted as A and B in Fig. 1(a), result from the interaction of the $5d(e_g)\Gamma_{8g}$ state with the $4f^5(^6H_J)$ and $4f^5(^6F_J)$core electron substates and can be described as $4f^5(^6H)-5d(e_g)^1\Gamma_{8g}$ and $4f^5(^6F)-5d(e_g)^1\Gamma_{8g}$, respectively. Consequently, the bands C and D result from the interaction of the $4f^5(^6H_J)$ core electron substates with the $5d(t_{2g})\Gamma_{8g}$ and $5d(t_{2g})\Gamma_{7g}$ states and can be described as $4f^5(^6H)-5d(t_{2g})^1\Gamma_{8g}$ and $4f^5(^6H)-5d(t_{2g})^1\Gamma_{7g}$, respectively. By analogy, bands E and F should be attributed to transitions to levels originating from the $4f^5(^6F)-5d(t_{2g})^1\Gamma_{8g}$ and $4f^5(^6F)-5d(t_{2g})^1\Gamma_{7g}$, respectively. Therefore, the splitting between bands C and D or between bands E and F, which is of the order of 1500–2000 cm^{-1}, results from the spin-orbit coupling of $5d$ electron.

The crystal-field splitting (10 Dq) of the $4f^5 5d^1$ configuration for $Sm^{2+}:SrCl_2$ may be evaluated experimentally as the energy difference between the $5d(t_{2g})$ levels (split by the spin-orbit coupling) and the $5d(e_g)$ levels, that is as the difference between the barricenter of bands C+D and band A or between the barricenter of bands E+F and band B. The thus obtained value of 10 Dq is in the 10 000–12 000 cm^{-1} range and is, as one might expect, about a factor of two smaller than the value of $\geq$20 000 cm^{-1} for the $5f^2 6d^1$ configuration of U^{3+} in the same host.[16]

This simple model, although strongly simplified, seems to properly account for the main structure of absorption bands observed in 15 000–35 000 cm^{-1} region. However, actually, the observed bands result from overlapping transitions to various levels arising from the $4f^5 5d^1$ configuration due to a range of interactions included in Hamiltonian of Eq. (1). The further details of bands assignment, pertinent to the results of CF calculations, are given in Section IV B.

In the 15 000–25 000 cm^{-1} range the fine structure of the absorption bands, which consists of phonon satellites coupled to the ZP lines, is clearly observed. Axe and Sorokin[18] suggested, that the mode responsible for the formation of the major 213 cm^{-1} vibrational progression observed in $Sm^{2+}:SrCl_2$ spectrum is e_g rather than a_{1g}. However, the reasoning presented in Ref. 17 points to a_{1g} as the more appropriate assignment, which is consistent with the *f-d* spectra of Ln^{3+} in CaF_2 (Ref. 11) and U^{3+} in $SrCl_2$ (Ref.

16). The $\nu_2 \sim 81$ cm^{-1} and $\nu_3 \sim 116$ cm^{-1}modes should be attributed either to $k=0$ t_{2g} modes at the zone boundary or to second shell motions.[17]

In the region above 25 000 cm^{-1} the vibronic pattern is not as clearly resolved as it is for the lower energy bands. This may partly results from the lower resolution of the spectrometer in the UV region, but more probably from the high density of overlapping ZP and phonon transitions, contributing to the observed spectral lines and causing their broadening.

From the theoretical model fit of the experimental spectrum (Sec. IV C) the value of 1.44–1.51 was obtained for the $S(a_{1g})$ Huang-Rhys parameter, which points to a rather weak electron-lattice coupling. A very similar value of $S(a_{1g}) \sim 1.5$ was derived for U^{3+} in $SrCl_2$ (Ref. 16), and a slightly smaller value of $S(a_{1g})=1.28$ for Eu^{2+} in the same host crystal.[17]

B. Hamiltonian parameters and $4f^5 5d^1$ energy levels

Since the number of experimentally determined energy levels is significantly smaller then the number of those predicted by the theory, and particularly no ZP could have been identified in the spectral region above 25 000 cm^{-1}, we minimized in the optimization procedure the differences between the overall experimental and calculated spectral profiles, instead of individual crystal-field components. Thus, the parameters of Hamiltonian of Eq. (1) were optimized to obtain the best possible agreement between the calculated and experimental barricenters as well as the relative intensities of the seven well separated bands, denoted in Fig. 1(a) as bands A–H. In this procedure a total of nine parameters were varied and determined simultaneously, and their final values are shown in Table II.

Because of the difference between the equilibrium distance of the metal ion and the ligand in the ground and excited states, resulting from the larger extent of $5d$ orbitals compared to the $4f$ orbitals, most of the transition intensity is in the vibronic bands. However, the simulation of the vibronic intensities for the bands situated above 25 000 cm^{-1} would be an overwhelming task due to the large number of zero-phonon transitions. Thus, in order to make a comparison with experiment, we simulated the whole unpolarized absorption spectrum of Sm^{2+}:$SrCl_2$ making a rough assumption that the vibronic sidebands coupled to each of the zero-phonon line may be approximated by a single broad Gaussian shape band. In simulation, this band is shifted from the ZP lines by 300 cm^{-1} with FWHM (full width at half maximum) of 650 cm^{-1} and its oscillator strength is proportional to the line strength calculated for a given ZP transition multiplied by the transition energy. The above values of displacement and width were chosen as giving the best fit to positions and shapes of experimental bands. The simulated absorption spectrum of Sm^{2+}:$SrCl_2$ is shown in Fig. 1(b). The agreement between the simulated and experimental spectrum is excellent, considering both the bands positions and their relative intensities. Even the low intensity bands observed between 17 500 and 23 000 cm^{-1} are well reproduced.

In order to compare the quality of the fit at the level of individual ZP lines, the correspondence between calculated positions of ZP lines [Fig. 1(b)] and thirteen experimental ZP lines determined in 15 000–25 000 region [Fig. 1(a)] is indicated by the dot vertical lines. The agreement is satisfactory, especially as for the calculations in which the parameters were optimized for the overall spectrum and not for the individual ZP transitions.

The bands observed in the lowest energy part of the spectrum are due to the transitions from the $4f^6(^7F_0)$ level to the $4f^5 5d^1$ configuration multiplets of the $(^6H)^7K_4+(^6H)^7F_1$ and $(^6H)^7K_5+(^6H)(^7G_1, ^7I_3)$ main characters. However, the bands observed at energy higher then 25 000 cm^{-1} results from overlapping transitions to numerous levels forming a dense array of energy states. In Fig. 1(b) are indicated the largest components of the eigenvectors for the terminal levels of the $4f^5 5d^1$ configuration, with the highest predicted $^7F_0 \rightarrow (S_f L_f)$ SLJ transition intensities within a given absorption band. Thus, the bands C and D [Fig. 1(a)] are mostly due to transitions to levels originating from the $(^6H)^7L_J$ multiplets, although in this spectral region transitions to the $(^6H)^5L_J$ and $(^6F)^5L_J$ also occur. The bands B, E, and F result predominantly from transitions to the levels originating from the $(^6F)^7L_J$ multiplets, overlapping with the less intense transitions to the $(^6H)^5L_J$ multiplets. At energy above 40 000 cm^{-1} transitions to levels resultant from the $(^6F)^5L_J$ and $(^6P)^7L_J$ multiplets as well as the quartet $(^4L_f)SLJ$ multiplets are observed. This energy levels diagram, emerging from the CF calculations, is in a general accordance with the scheme obtained from the qualitative reasoning based on the simple model, presented in Sec. IV A.

The bands predicted at energy higher then 45 000 cm^{-1} have not been recorded experimentally. However, since there is a very good agreement between the model spectrum and the spectrum measured in the range experimentally available, one may expect that the positions and intensities of the unobserved bands are calculated with a similarly good accuracy.

In the final fit, we have adjusted values of nine parameters, given in Table II. The optimized values of $F^2(ff)$ and $\zeta_{4f}(ff)$ parameters for $4f^5 5d^1$ configuration are close to the values for $4f^5$ configuration of Sm^{3+}. Analogous trend is observed for U^{3+} ions in $SrCl_2$, where the determined values of the $F^k(ff)$ and $\zeta_{5f}(ff)$ parameters for the $5f^2 6d^1$ configuration are similar to those typical for the $5f^2$ configuration of U^{4+} in a chloride environment.[16] The similar relation also results from calculations using Cowan's code—the free-ion values of $F^k(ff)$ parameters for the $4f^5 5d^1$ configuration are placed between the values for the $4f^6$and $4f^5$ configurations, but are significantly closer to the latter one.

The values obtained for the direct, $F^k(fd)$, and exchange, $G^j(fd)$, Coulomb f-d interaction parameters are 58.1% and 61.1% of the free ion values, respectively. This reduction is noticeably larger compared to that for Ln^{3+} ions, in which these parameters were typically reduced to about 67% of their *ab initio* calculated free-ion values.[11] Such trend is expected, because a larger reduction of f-d interaction parameters is anticipated for the larger Sm^{2+} ion, with the more covalent metal-ligand bonds. Accordingly, for Eu^{2+} in $SrCl_2$

the values obtained for the *f-d* Coulomb interaction parameters are ~49% of the free-ion values.[17] Even larger reduction of $F^2(fd)$ parameter, to 38.6% of free-ion value, is observed for U^{3+} ion in $SrCl_2$ (Ref. 16), and may be linked to the larger extension of $5f$ and $6d$ orbitals with respect to the $4f$ and $5d$ orbitals.

The adjusted in the optimization procedure value for the $B_0^4(dd)$ crystal-field parameter of the $5d$ electron equals to $-20\,500$ cm^{-1} and is similar to the value of $-21\,296$ cm^{-1} derived for Eu^{2+} in $SrCl_2$ (Ref. 17).

C. Simulation of $4f^6 \rightarrow 4f^5 5d^1$ transition vibronic spectrum

The simulation of vibronic spectrum was performed for three well resolved bands observed in the lowest energy region of the absorption spectrum, shown in detail in Fig. 3(a). The bands observed in the 15 200–16 200 cm^{-1} (band A–I) and 18 000–19 000 cm^{-1} (band A–III) spectral range are composed of vibronic structure built on the single electronic origins at 15 280 cm^{-1} [ZP(1)] and 18 018 cm^{-1} [ZP(6)], respectively. The intense massive labeled as A-II, observed between 16 250 and 17 250 cm^{-1}, results from the overlapping vibronic sidebands coupled to three ZP lines at 16 268 [ZP(2)], 16 297 [ZP(3)] and 16 743 [ZP(4)] cm^{-1}. The very weak electronic origin, ZP(5), which may be noticed at 17 300 cm^{-1}, and its vibronic envelope, were not included into simulation.

To reproduce the features of experimental spectrum we assumed that they result from the electronic $4f^6 \rightarrow 4f^5 5d^1$ transitions coupled to the three local vibrational modes at $h\omega_1 \sim 213$ cm^{-1}, $h\omega_2 \sim 115$ cm^{-1} and $h\omega_3 \sim 81$ cm^{-1}. The contributions of up to fourth order of harmonics and frequency summation of various orders of the ω_1, ω_2, and ω_3 frequencies, were also allowed. The relative intensities of vibronic lines observed for *n*th progression suggest the expected value of the Huang-Rhys constant of about 1.5 for $h\omega_1$ mode, and less than 1 for other modes.

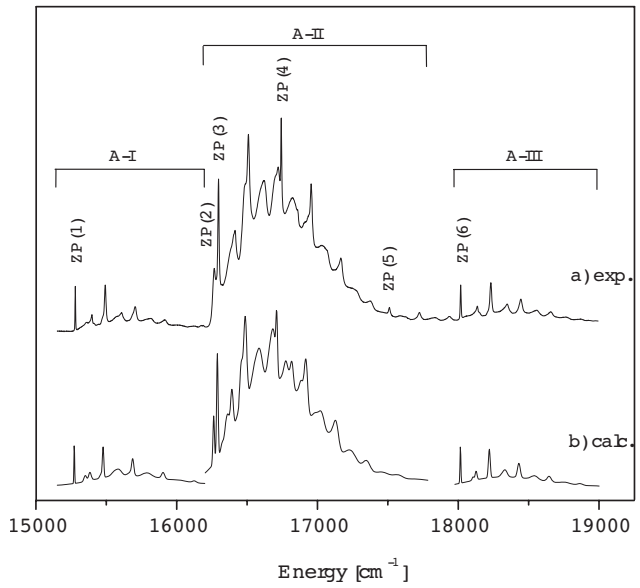

FIG. 3. Experimental (a) and calculated (b) absorption spectra for the multiphonon vibronic transitions between the ground $^7F_0$ level of the $4f^5$ configuration and the lowest levels of $4f^5 5d^1$ configuration, observed in the 15 250–19 000 cm^{-1} energy range. The low intensity ZP(5) line and its vibronic satellites were not included in modeling.

Below the narrow peaks the broad band extending for a few hundred of cm^{-1} is observed in the spectrum. The occurrence of this broad background may be attributed to the contributions from coupling to the lattice acoustic modes.[24,25] In the modeling of the spectrum the broad background may simulated by independent term in the line shape function, in which an average lattice frequency ω_0 and a relatively large bandwidth σ_0 is introduced.

For the simulation of the overall profile of the multi-mode and multiphonon vibronic spectrum of $4f^6 \rightarrow 4f^5 5d^1$ transitions, a spectral function developed in Ref. 25 was employed:

$$F(E) = F_{\text{latt}} \sum_{K=0}^{\infty} \frac{\exp[-S_0] S_0^K}{K!} \frac{1}{(2\pi\sigma_0^2)^{1/2}} \exp\left[\frac{-(E_{\text{ZPL}} - E - K\hbar\omega_0)^2}{2\sigma_0^2}\right]$$
$$+ F_{loc} \sum_{L=0}^{4} \sum_{M=0}^{4} \sum_{N=0}^{4} \frac{\exp[-S_1 - S_2 - S_3] S_1^L S_2^M S_3^N}{L!\,M!\,N!} \frac{1}{\{2\pi[(L+1)\sigma]^2\}^{1/2}} \times \exp\left[\frac{-(E_{\text{ZPL}} - E + L\hbar\omega_1 + M\hbar\omega_2 + N\hbar\omega_3)^2}{2[(L+1)\sigma]^2}\right] \quad (2)$$

where S_0 and $S_{1,2,3}$ are the Huang-Rhys factors for the average lattice and the three local vibrational modes with the frequencies ω_0 and $\omega_{1,2,3}$, respectively; σ_0 and σ are the widths of the individual phonon lines of Gaussian shape for the average lattice mode and the three local modes, respectively; and E_{ZPL} is the zero-phonon line energy.

The analysis of experimental spectrum reveals that the vibronic lines of higher progressions become successively broader. For example, the FWHM of ZP(1) line at 15 280 cm^{-1} is equal to 5.2 cm^{-1}, whereas the FWHM of ZP(1)+$h\omega_1$ (15 492 cm^{-1}) and ZP(1)+$2h\omega_1$ (15 705 cm^{-1}) phonon lines equals to 12.6 and 19.6 cm^{-1}, respectively. To account for this broadening, in the line shape function of Eq. (2) the widths of the L (L=0–4) series of harmonic lines of Gaussian shape are multiplied by a factor of L+1. Moreover, the widths of the phonon lines for $h\omega_2 \sim 81$ cm^{-1}(σ_2) and

TABLE III. Parameters of the line shape function of Eq. (2) for the $4f^6-4f^55d^1$ transitions of Sm^{2+} in $SrCl_2$.

	Value		
Parameter	Band A–I[a]	Band A–II[a]	Band A–III[a]
$E_{ZPL}(1)$	15 279.9±0.1 cm^{-1}	16 268.0±0.4 cm^{-1}	18 018.0±0.1 cm^{-1}
$E_{ZPL}(2)$		16 297.0±0.2 cm^{-1}	
$E_{ZPL}(3)$		16 743.0±0.3 cm^{-1}	
S_1	1.49±0.03	1.66±0.03	1.44±0.02
S_2	0.70±0.05	0.71±0.03	0.52±0.02
S_3	0.51±0.05	0.28±0.03	0.19±0.02
$h\omega_1$	212.6±0.2 cm^{-1}	212.2±0.3 cm^{-1}	213.6±0.1 cm^{-1}
$h\omega_2$	115.7±0.8 cm^{-1}	111.2±0.6 cm^{-1}	115.6±0.4 cm^{-1}
$h\omega_3$	81.4±0.7 cm^{-1}	65±1 cm^{-1}	91±1 cm^{-1}
σ_1	2.57±0.06 cm^{-1}	5.8±0.1 cm^{-1}	3.24±0.05 cm^{-1}
σ_2	9.2±0.6 cm^{-1}	10.4±0.4 cm^{-1}	7.3±0.3 cm^{-1}
σ_3	9.2±0.6 cm^{-1}	10.4±0.4 cm^{-1}	7.3±0.3 cm^{-1}
S_0	3.1±0.2	3.38±0.05	2.4±0.3
$h\omega_0$	140±10 cm^{-1}	140±2 cm^{-1}	164±19 cm^{-1}
σ_0	82±20 cm^{-1}	75±4 cm^{-1}	128±24 cm^{-1}

[a]Bands labels correspond to those in Fig. 3(a).

$h\omega_3 \sim 115$ cm^{-1} (σ_3) modes were assumed to be the same ($\sigma_2=\sigma_3$), but they were allowed to be different from the width of that for the $h\omega_1 \sim 213$ cm^{-1} (σ_1) mode. Thus, in Eq. (2) $\sigma=\sigma_1$ for $M=0$ and $N=0$ (which corresponds to ZP lines and ZP+$Lh\omega_1$ phonon lines), and $\sigma=\sigma_2=\sigma_3$ otherwise.

A non linear least-square fitting of Eq. (2) to the experimental absorption spectrum was carried out and the parameters obtained from this procedure are listed in Table III. The model calculated spectrum is plotted in Fig. 3(b).

One may state that a very good agreement between the experimental and calculated spectra was achieved, with the consistent values of the optimal spectral function parameters resulted for the three independently fitted bands. It is worth to notice that the very satisfactory results were obtained not only for the A-I and A-III vibronic bands, arising from the single electronic origins, but also for a relatively composed A-II vibronic massive, consisting of overlapping vibronic satellites accompanying the three ZP lines.

The dimensionless Huang-Rhys parameter S is related to the displacement ΔQ_k along the nuclear coordinate Q_k of mode k as follows: [26]

$$S_k = \frac{\pi C \bar{\nu}_k \mu}{\hbar} (\Delta Q_k)^2 \tag{3}$$

where $\bar{\nu}_k$ is frequency of a vibrational mode (in [cm^{-1}]) and μ is the reduced mass. For $S(a_{1g})=1.46$ and $\bar{\nu}(a_{1g})=213.1$ cm^{-1} values, obtained by averaging parameters derived for A–I and A–III bands (Table III), and $\mu(a_{1g})=m(\mathrm{Cl})$, we obtain from Eq. (3) the absolute equilibrium displacement $|\Delta Q(a_{1g})|=0.114$ Å. This corresponds to the Sm-Cl bond length difference $|\Delta R_{\mathrm{Sm\text{-}Cl}}(a_{1g})|$ between the ground $4f^6$ and first excited $4f^55d^1$ state of $|\Delta R_{\mathrm{Sm\text{-}Cl}}(a_{1g})| = |\Delta Q(a_{1g})|/\sqrt{8}=0.04$ Å. From this analysis it is not possible to determine the sign of $\Delta R_{\mathrm{Sm\text{-}Cl}}(a_{1g})$. However, the results of the quantum mechanical calculations[27] indicate that for lanthanide and actinide ions in sixfold octahedral and eightfold cubic complexes the bond length between metal ion and the surrounding ligands shorten upon $nf^N \rightarrow nf^{N-1}(n+1)d^1$ excitations. Thus, we can safely assume that the $4f^6 \rightarrow 4f^55d^1$ excitation of Sm^{2+} in $SrCl_2$ is accompanied by the Sm-Cl bond decrease by about 0.04 Å.

V. CONCLUSIONS

In this paper, a low-temperature $4f^6 \rightarrow 5f^56d^1$ absorption spectrum of Sm^{2+} in $SrCl_2$ single crystals, recorded in the spectral range extended to 45 000 cm^{-1}, has been presented. In the region above 25 000 cm^{-1} a number of absorption bands, to our knowledge not reported so far in the literature, has been identified, among them those resulting from transitions to the $4f^55d^1(t_{2g})$ levels. Taking into account the good quality of the recorded spectrum, with the well separated bands observed in a broad spectral range, as well as a very well resolved fine vibronic structure for transitions between the 15 000 and 25 000 cm^{-1}, one may state that this spectrum provides some of the most abundant experimental information on f-d spectra, as compared to other hitherto reported for Ln^{3+} or Ln^{2+} ions.

The predominant phonon line observed in the spectrum corresponds to a ~ 213 cm^{-1} $\nu_1(a_{1g})$ stretching mode. The value of $S(a_{1g}) \sim 1.5$ determined for the Huang-Rhys parameter points to a relatively weak electron-lattice coupling. Besides the totally symmetric mode, the two other vibronic modes, at ~ 81 cm^{-1} and ~ 116 cm^{-1}, are recognized in the

spectrum. From an analysis of the vibronic structure 13 zero-phonon lines, corresponding to transitions from the $^7F_0$ ground multiplet of the $4f^6$ configuration to the $4f^5 5d^1(e_g)$ levels, were assigned between 15 000 and 25 000 cm^{-1}.

Energy-level calculations for the $4f^5 5d^1$ configuration of Sm^{2+} have been performed using a theoretical model for nf^N energy levels extended for interactions related with the presence of *d*-electron and the overall $4f^6 \rightarrow 5f^5 6d^1$ absorption spectrum has been very satisfactorily reproduced. The calculations predict some lower intensity bands, at energy between 45 000 and 55 000 cm^{-1}, which spread beyond the region of the recorded experimental spectrum. The optimized values of $F^2(ff)$ and $\zeta_{4f}(ff)$ parameters for the $4f^5 5d^1$ configuration are close to those for the $4f^5$ configuration of Sm^{3+}. The direct, $F^k(fd)$, and exchange, $G^j(fd)$, Coulomb *f-d* interaction parameters are reduced to about 60% of the free ion values.

The vibronic structure observed in the spectra is adequately reproduced using the theory of multiphonon vibronic coupling to electronic transitions. It is assumed that the sharp vibronic sidebands result from the coupling to three local modes, whereas the lattice mode induces a broad background. The fitting of experimental vibronic spectrum have been performed for the three well resolved absorption bands in 15 000–19 000 cm^{-1} region and the consistent parameters of the vibronic line shape function for *f-d* transitions of $Sm^{2+}:SrCl_2$ have been determined. On the basis of the determined value of the Huang-Rhys parameter the shortening of the Sm-Cl bond by about 0.04 Å upon the $4f^6 \rightarrow 4f^5 5d^1$ excitation was deduced.

*Corresponding author: karb@wchuwr.pl

[1] B. G. Wybourne, *Spectroscopic Properties of Rare Earths* (Interscience, New York, 1965).
[2] D. J. Newman and B. Ng (eds.), *Crystal Field Handbook* (Cambridge University Press, Cambridge, 2000).
[3] W. T. Carnall, *ANL-89/39 report* (Argonne National Laboratory, Chicago, 1989).
[4] J. Sytsma, D. Piehler, N. M. Edelstein, L. A. Boatner, and M. M. Abraham, Phys. Rev. B **47**, 14786 (1993).
[5] M. Marsman, J. Andriessen, and C. W. E. van Eijk, Phys. Rev. B **61**, 16477 (2000).
[6] L. L. Chase, Phys. Rev. B **2**, 2308 (1970).
[7] A. Weakliem, Phys. Rev. B **6**, 2743 (1972).
[8] K. E. Johnson, and J. N. Sandoe, J. Chem. Soc. A **1969**, 1694.
[9] B. Ordejón, M. Karbowiak, L. Seijo, and Z. Barandiarán, J. Chem. Phys. **125**, 074511 (2006).
[10] F. Ruiperez, Z. Barandiarán, and L. Seijo, J. Chem. Phys. **123**, 244703 (2006).
[11] M. F. Reid, L. van Pieterson, R. T. Wegh, and A. Meijerink, Phys. Rev. B **62**, 14744 (2000).
[12] L. van Pieterson, M. F. Reid, R. T. Wegh, S. Soverna, and A. Meijerink, Phys. Rev. B **65**, 045113 (2002).
[13] L. van Pieterson, M. F. Reid, G. W. Burdick, and A. Meijerink, Phys. Rev. B **65**, 045114 (2002).
[14] L. Ning, Y. Iiang, S. Xia, and P. A. Tanner, J. Phys.: Condens. Matter **15**, 7337 (2003).
[15] M. Karbowiak, Chem. Phys. **314**, 189 (2005).
[16] M. Karbowiak, J. Phys. Chem. A **109**, 3569 (2005).
[17] Z. Pan, L. Ning, B.-M. Cheng, and P. A. Tanner, Chem. Phys. Lett. **428**, 78 (2006).
[18] J. D. Axe and P. P. Sorokin, Phys. Rev. **130**, 945 (1963).
[19] Y. Y. Yeung, M. F. Reid, and D. J. Newman, Appendix 3: Accessible program packages, edited by D. J. Newman and B. Ng in *Crystal Field Handbook* (Cambridge University Press, Cambridge, 2000), pp. 254–258.
[20] C. Görller-Walrand and K. Binnemans, Rationalization of Crystal-Field Parametrization, edited by K. A. Gschneidner, Jr. and L. Eyring *Handbook on the Physics and Chemistry of Rare Earths*, Vol. 23 (Elsevier Science B.V, Amsterdam, 1996).
[21] K. Lesniak, J. Phys.: Condens. Matter **2**, 5563 (1990).
[22] R. D. Cowan, *The Theory of Atomic Structure and Spectra* (University of California Press, Berkeley, 1981).
[23] R. D. Shannon, Acta Crystallogr. **32**, 751 (1976).
[24] M. Wagner and W. E. Bron, Phys. Rev. **139**, A233 (1965).
[25] G. K. Liu, X. Y. Chen, N. M. Edelstein, M. F. Reid, and J. Huang, J. Alloys Compd. **374**, 240 (2004).
[26] B. Henderson, G. F. Imbush, *Optical Spectroscopy of Inorganic Solids* (Oxford Science Publications, Oxford, 1989).
[27] Z. Barandiarán and L. Seijo, Theor. Chem. Acc. **116**, 505 (2006).